Gravity effect of water storage changes in a weathered hard-rock aquifer in West Africa: results from joint absolute gravity, hydrological monitoring and geophysical prospection

Basile Hector, Luc Séguis, Jacques Hinderer, M. Descloitres, J.M. Vouillamoz, M. Wubda, Jean-Paul Boy, Bernard Luck, Nicolas Le Moigne

Geophysical Journal International

Geophys. J. Int. (2013) **194,** 737–750
Advance Access publication 2013 April 30

doi: 10.1093/gji/ggt146

Gravity effect of water storage changes in a weathered hard-rock aquifer in West Africa: results from joint absolute gravity, hydrological monitoring and geophysical prospection

Basile Hector,[1] Luc Séguis,[2] Jacques Hinderer,[1] Marc Descloitres,[3] Jean-Michel Vouillamoz,[3] Maxime Wubda,[3] Jean-Paul Boy,[1] Bernard Luck[1] and Nicolas Le Moigne[4]

[1] *IPGS-EOST, CNRS/UdS, UMR* 7516, 5 *rue René Descartes,* 67084 *Strasbourg Cedex, France. E-mail: basile.hector@unistra.fr*
[2] *IRD/CNRS/UM2/UM1, UMR HydroSciences Montpellier, Place E. Bataillon, F-*34095 *Montpellier Cedex* 5, *France*
[3] *IRD/UJF-Grenoble-*1*/CNRS/G-INP – UMR LTHE,* 08 *BP* 841 *Cotonou, Benin*
[4] *Géosciences Montpellier, UMR CNRS/UM2* 5243, *Montpellier, France*

Accepted 2013 April 9. Received 2013 April 8; in original form 2012 August 19

SUMMARY

Advances in groundwater storage monitoring are crucial for water resource management and hydrological processes understanding. The evaluation of water storage changes (WSC) often involve point measurements (observation wells, moisture probes, etc.), which may be inappropriate in heterogeneous media. Over the past few years, there has been an increasing interest in the use of gravimetry for hydrological studies. In the framework of the GHYRAF (Gravity and Hydrology in Africa) project, 3 yr of repeated absolute gravity measurements using a FG5-type gravimeter have been undertaken at Nalohou, a Sudanian site in northern Benin. Hydrological data are collected within the long-term observing system AMMA-Catch. Once corrected for solid earth tides, ocean loading, air pressure effects, polar motion contribution and non-local hydrology, seasonal gravity variations reach up to 11 μGal, equivalent to a WSC of 260-mm thick infinite layer of water. Absolute temporal gravity data are compared to WSC deduced from neutron probe and water-table variations through a direct modelling approach. First, we use neutronic measurements available for the whole vertical profile where WSC occur (the vadose zone and a shallow unconfined aquifer). The RMSD between observed and modelled gravity variations is 1.61 μGal, which falls within the error bars of the absolute gravity data. Second, to acknowledge for the spatial variability of aquifer properties, we use a 2-D model for specific yield (Sy) derived from resistivity mapping and Magnetic Resonance Soundings (MRS). The latter provides a water content (θ_{MRS}) known to be higher than the specific yield. Hence, we scaled the 2-D model of θ_{MRS} with a single factor (α). WSC are calculated from water-table monitoring in the aquifer layer and neutronic measurements in the vadose layer. The value of α is obtained with a Monte–Carlo sampling approach, minimizing the RMSD between modelled and observed gravity variations. This leads to $\alpha = Sy/\theta_{\mathrm{MRS}} = 0.63 \pm 0.15$, close to what is found in the literature on the basis of pumping tests experiments, with a RMSD value of 0.94 μGal. This hydrogeophysical experiment is a first step towards the use of time-lapse gravity data as an integrative tool to monitor interannual WSC even in complicated subsurface distribution.

Key words: Time variable gravity; Hydrogeophysics; Hydrology; Africa.

1 INTRODUCTION

Water Storage Changes (WSC) in unsaturated soils and aquifers are a key variable for water resource management, yet still challenging to estimate (Scanlon *et al.* 2002; Healy & Scanlon 2010; Dubus & Dubus 2011). This is particularly true in the weathered hard-rock basement of the Sudanian zone in West–Africa, where the total storage volume is low, but shows strong annual variations (MacDonald *et al.* 2012). There, urban development relies on the ability to provide enough fresh water along the year through high yield boreholes. These are still difficult to implement and the knowledge of local recharge is particularly important for their sustainability.

For instance, in the surroundings of the Nikki town in the hard-rock area of northern Benin, half of the boreholes drilled in 2011 were considered as dry (Direction Générale de l'Eau, Cotonou, personal communication, 2012), despite a high mean annual rainfall of 1300 mm. Furthermore, Achidi *et al.* (2012) found a 62 per cent success rate for water drillings in crystalline basement at the country scale, against up to 90 per cent for coastal sedimentary aquifers. Seasonal WSC is thus of critical concern in this highly sensitive area, and broadening the range of methods available to monitor this key variable is a major challenge.

There are numerous approaches for the evaluation of WSC that are usually based on distributed (or not) point measurements in one or several compartments responsible for WSC [i.e. top soil, vadose zone (VZ), water tables]. For instance, Time-Domain Reflectometry (TDR) is now widespread for water content monitoring, but has several limitations such as the small sampling volume (10^{-3} m^3) of a single measurement and its limitation to the upper layers of the VZ. Deriving WSC from water-table monitoring strongly depends on the knowledge of the specific yield (Sy) parameter, and only provides WSC for the water-table fluctuation zone (WTFZ). Geophysical methods are often used to characterize underground structures for extending these point measurements. WSC at the field scale can be estimated by the interpolation of these point measurements, or by several methods such as water budget estimations or numerical modelling (Healy & Cook 2002; Scanlon *et al.* 2002). As noticed by Creutzfeldt *et al.* (2010b), Christiansen *et al.* (2011b) and several others, deriving WSC from limited point measurements is still an arduous task, despite recent developments that are often limited to the upper layers of the ground (spatial TDR measurements, high-precision lysimeters, cosmic ray neutron probes, etc.). This led some open space for the emerging hydrogravimetry method which allows to perform direct non-invasive monitoring that can be derived into integrative WSC estimations if other components affecting gravity are correctly removed (Pfeffer *et al.* 2011).

Water mass redistribution leads to variations in the Earth's gravity field, which can be measured by gravimeters. Superconducting Gravimeters (SGs) provide continuous relative gravity monitoring with very high accuracy (about 1 nm s^{-2}). Apart from very recent developments on new SGs, they are drift-prone and can hardly be moved, which are their main drawbacks for hydrological studies. For further details on SGs, see for instance Goodkind (1999) and Hinderer *et al.* (2007). Spring-based gravimeters are lower accuracy (few μGal) relative gravimeters for field prospecting. They give access to spatial gravity variations with respect to a base station, and can thus provide spatiotemporal variations with repeated measurements (Naujoks *et al.* 2008; Jacob *et al.* 2010; Pfeffer *et al.* 2013). Their lower accuracy puts them on the edge of detection for many hydrological cases for which much care must be taken to achieve the best results, leading to a second drawback, the time consumption. However, they can be a powerful tool when used together with a SG or an absolute gravimeter (AG) as a base station. AGs have the advantage to be drift-free, allowing for monitoring gravity changes at long timescales, by repeating measurements without leaving the instrument at the same place. They give direct measurements of the earth gravity field with a 10–20 nm s^{-2} (1–2 μGal) precision for the most accurate one, the FG5 model (Niebauer *et al.* 1995). The FG5 AG measures the successive positions of a free falling corner cube in a vacuum chamber, using a laser interferometer and an atomic clock. The actual gravity value along the direction of the local vertical is obtained for every drop.

Until recently, the hydrological signal has mainly been seen by the geodesy community as 'noise' to be removed from the SGs time-series—often calibrated with absolute gravity measurements—to recover small geodynamics signals. Many site-specific hydrogravimetric studies can be found in the literature (e.g. Bower & Courtier 1998; Harnisch & Harnisch 2006; Imanishi *et al.* 2006; Kroner & Jahr 2006; Van Camp *et al.* 2006; Creutzfeldt *et al.* 2008; Longuevergne *et al.* 2009; Creutzfeldt *et al.* 2010a,b; Naujoks *et al.* 2010). However, only very few studies use AGs as field instruments for measuring temporal changes due to the redistribution of water (Jacob 2009; Pfeffer *et al.* 2011). This allows to investigate other areas than single SGs observatories without being affected by the drift and accuracy limitations of the microgravimeters.

Gravity measurements are often compared to hydrological monitoring, by calculating the gravity effect of these measured WSC in a direct modelling approach (Creutzfeldt *et al.* 2008; Jacob *et al.* 2008; Creutzfeldt *et al.* 2010a; Pfeffer *et al.* 2011). A few recent studies also successfully calibrated conceptual or physical hydrological models in a coupled hydrogeophysical inversion framework such as defined by Ferré *et al.* (2009) (see also Creutzfeldt *et al.* 2010b; Christiansen *et al.* 2011a,b). However, to successfully compare gravity data and hydrological monitoring, the hydrogravimetry method is also limited by the poor spatial extent of hydrological point measurements, and by the integrative character of gravity data. The latter requires some knowledge of the WSC of each compartment in the footprint area of the gravimeter. Very few studies consider the contribution of each layer, and the VZ is usually poorly or not documented (Christiansen *et al.* 2011b). Creutzfeldt *et al.* (2010a) presented the first study which comprehensively measured WSC in all relevant storage components, namely groundwater, saprolite, soil, topsoil and snow storage, and compared them to gravity measurements.

A usual byproduct of hydrogravimetric surveys is an estimation of the specific yield (Sy) parameter, as it relates water-table fluctuations (an observation easily available) to unconfined aquifer storage variations. This can be done for various levels of precision, using relative spring-based gravimeters (Montgomery 1971; Pool & Eychaner 1995; Gehman *et al.* 2009), absolute gravity data (Jacob *et al.* 2008; Pfeffer *et al.* 2011) or even GRACE (Gravity Recovery and Climate Experiment) satellite products (Shamsudduha *et al.* 2012). However, Creutzfeldt *et al.* (2010a) pointed out that 'interpreting the regression coefficient [between gravity and water table level] in a physical way is problematic and only valid if the correlation between groundwater and other water storages can be neglected or the water mass variations in all other storages are small compared to the groundwater mass variation'. One may also add that the assertion is valid if WSC in other storages are known and their gravity effect can be calculated and removed from the regression analysis. At the field scale, Sy estimates are derived from classical hydrological experiments such as pumping tests or water budgets estimates. More recently, the emerging geophysical method of Magnetic Resonance Soundings (MRS) which determines a 'MRS water content' parameter (θ_{MRS}) was also used for estimating Sy (Healy & Cook 2002; Vouillamoz *et al.* 2005; Boucher *et al.* 2009). Comparing Sy obtained from pumping tests to θ_{MRS}, these authors observed lower Sy values with respect to θ_{MRS}, as summarized by the study of Vouillamoz *et al.* (2012) who found $Sy/\theta_{\mathrm{MRS}} = 0.4$ for a clayey sandstones aquifer in Northern Cambodia.

In this paper, we present an AG survey carried out in a tropical weathered hard-rock unconfined aquifer context of subhumid West Africa (Nalohou, Benin: 1.6056°E–9.7424°N) during 3 yr (2009–2011) using high accuracy FG5 measurements (four measurements a year). These measurements have been carried out in the framework of the GHYRAF (Gravity and HYdRology in AFrica) project that

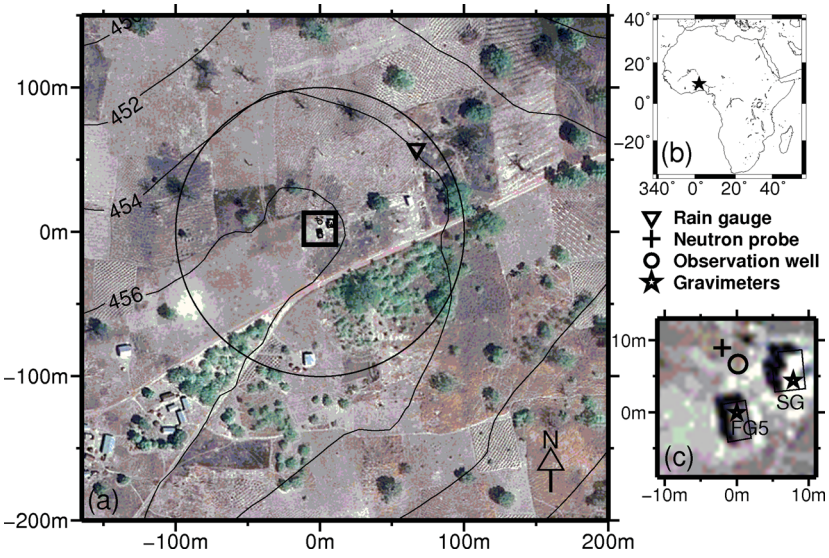

Figure 1. Study area, measurement settings: gravimeters (FG5 and SG) and their shelters. Neutron probe borehole and observation well are respectively located 9 and 7 m to the FG5 location. The circle shows the 100-m radius zone of influence for gravity variations at the FG5 site. *Google Earth* image, 2010 February 4.

aims at evaluating the ability of AGs to measure water storage variations in West Africa (Hinderer *et al.* 2009; Hinderer *et al.* 2012). This project studies the strong seasonal monsoon signal within different aquifers (sedimentary in Niger and weathered hard rock in Benin) and climatic contexts (Sahelian and Sudanian zones). We also used the intensive hydrological monitoring that has been carried out at Nalohou site since 1992 in the frame of the AMMA-Catch long-term observing system (www.amma-catch.org; Lebel *et al.* 2009), which is an observatory of RBV (Réseau des Bassins Versants), the French critical zone exploration network (rnbv.ipgp.fr). The data are available upon request via the AMMA-Catch online database (http://database.amma-international.org/).

The objective of this study is to compare absolute gravity monitoring with seasonal WSC deduced from independent hydrological data (neutronic measurements and water-table levels). This is achieved through a direct modelling of the gravity variations induced by WSC. First, we evaluate the observed gravimetric variations against an integrative WSC model obtained with neutronic measurements from a single borehole that samples the whole profile (from surface down to the lowest level of the water table). Secondly, in order to take into account the spatial variability of Sy in this weathered hard-rock context, we distinguish between two layers to calculate the WSC: a shallow layer never saturated where WSC are deduced from neutron probe (NP) measurements and a deep layer where we use water-table data and a spatial distribution of Sy. The 2-D model for Sy is obtained by coupling resistivity mapping and MRS measurements that are scaled with a simple factor (α). The value of α is obtained with a Monte–Carlo sampling approach, minimizing the RMSD between modelled and observed gravity variations.

2 STUDY AREA

The Upper-Ouémé catchment in northern Benin (14 000 km^2) is a humid Sudanian area. It has been chosen for hydrological monitoring and accurate water budget estimations in the frame of the AMMA-Catch multidisciplinary project. A dense monitoring network dedicated to water redistribution processes studies has been developed since 2003 on a small, embedded, microcatchment close to the village of Nalohou (22.6 ha, Fig. 1), well suited for gravity measurements (Hinderer *et al.* 2012). Mean annual rainfall is 1195 mm yr^{-1} (over the period 1950–2004) at the Djougou weather station—8 km from the Nalohou site—(Kamagaté *et al.* 2007) and mean annual reference evapotranspiration is 1393 mm (over the period 2002–2006 at the Djougou weather station; Séguis *et al.* 2011). The Nalohou site has been equipped with observation boreholes (water table and neutronic measurements) and complementary geophysical surveys (electrical methods, MRS) have been undertaken. This contributed to some understanding of the prevailing hydrological processes and first estimates of the hydrological budget terms: the two main terms of the annual water budget are evapotranspiration (75–90 per cent of total rainfall amount) and streamflow (10–15 per cent). The residual term forms the interannual underground water storage variation (Kamagaté *et al.* 2007; Guyot *et al.* 2009; Descloitres *et al.* 2011; Séguis *et al.* 2011).

The unconfined aquifer is located in a weathered layer 7–22 m thick (Kamagaté *et al.* 2007; Descloitres *et al.* 2011) over a fresh metamorphic basement (gneiss, micaschists, quartzites). Geological structures are north–south oriented, and the mean dip angle is 20° east. Regional soils are of ferruginous tropical leached type, but slightly vary depending on the topography and local basement. Groundwater recharge occurs by direct infiltration of rainfall water through the VZ during the rainy season.

The land cover in the vicinity of the gravimeter is governed by crop (maize, sorghum, manioc and yam) and fallow rotations with some remaining trees (*Parkia biglobosa, vitellaria paradoxa*, *adansonia digitata*) kept for consumption purposes and a small cashew trees (*Anacardium occidentale)* orchard. Fallow is composed by trees (e.g. *Isoberlinia Doka*) and herbaceous cover, and the latter is usually burnt at the beginning of the dry season.

FG5 measurements are undertaken within a 3 × 4 m^2 shelter, close to another shelter for the SG. NP borehole and observation well (OW) are respectively located 9 and 7 m to the FG5 location (Fig. 1c). FG5 measurement site is located on the crest of a gentle sloping hill as shown by contour lines (Fig. 1a).

Except for large towns (such as nearby Djougou), the socioeconomical activity of the region is mainly rural, and the population density is close to 30 inhabitants per km^2, with an annual growth

of 3.48 per cent (1992–2002; Direction des études démographiques 2003). As there is almost no irrigation (rain-fed crops) so far, water consumption is mainly domestic, through the use of village wells, and is negligible in the water budget (about 0.2 mm yr^{-1}, on a basis of 20l per inhabitant per day; Séguis *et al.* 2011).

3 HYDROMETEOROLOGICAL MONITORING

Rainfall is monitored by a tipping-bucket raingauge located 100 m away from the FG5 measurement site (Fig. 1a). Cumulative and daily rainfall are shown on Fig. 2b and exhibit the seasonal rainfall pattern characteristic of the West African monsoon with wet and dry seasons. About 60 per cent of the total annual amount falls between July and September (Kamagaté *et al.* 2007). The interannual variability of rainfall is very marked in this area (e.g. Le Barbé *et al.* 2002; Le Lay & Galle 2005), and explains the divergence of these annual rainfall amounts with the mean calculated over a longer period (see section Study area), especially for 2009 and 2010 which were two particularly wet years.

Water table is measured every 2 d in a 10 m-deep OW at about 7 m of the FG5 measurement site since 2009 March (Fig. 1c). Other OWs located in the surroundings show similar variations in amplitude and phase. WSC in the WTFZ ($WSC_P, [L]$) are linked to water-table variations ($\Delta h, [L]$) through the specific yield Sy, using

$$WSC_P = Sy\Delta h. \quad (1)$$

Water-table time-series is shown in Fig. 2a. Maximal water-table depth occurs at the end of June/early July and is 6.3 m in average. The increase of minimum storage from 2008 to 2010 is probably linked to an early start of the rainy season and high annual rainfall in 2009 and 2010 as shown in Fig. 2(b). The late onset of the rainy season in 2011, after the wet year of 2010 is responsible for the drop in the minimum storage in 2011 June. These observations clearly show important interannual storage variations. Note that the thickness of the never-saturated VZ is about 1.7 m. From September to the following June, the groundwater depletion rate is regular and slow (12 mm d^{-1}). It has been shown that permanent groundwater does not drain into rivers through baseflow, instead groundwater depletion during the dry season (as in Fig. 2a) is more likely explained by root water uptake, even if deep drainage through fracture zones has not been discarded so far (Séguis *et al.* 2011). Another borehole located about 100 m from the gravimeter shows very similar water-table variations (less than 10 cm difference for the seasonal amplitude of about 4 m for the years 2009–2010, and much more, about 70 cm for the much drier year 2011—not presented in the study—and for which we suspect some problems). Another borehole also located about 100 m from the gravimeter, does exhibit similar water-table variations (less than 30 cm difference on the seasonal amplitude). This indicates that there are some small spatial variations of the water table, yet not directly linked to the topography or to a possible base level.

4 WATER STORAGE MONITORING

4.1 Method

About 9 m close to the OW is another 7.5-m deep borehole, but enclosed at its bottom, in which weekly measurements of soil moisture [θ,(%)] by NP are undertaken since 2009 March. For further details on NPs, the reader is referred to the IAEA training courses (IAEA 2003). Neutronic measurements are neutron counts measured in each layer of material and normalized by neutron counts acquired in the standard medium, that is, a water tank, giving counting rates (CR). Calibration is needed to transform these counting rates into

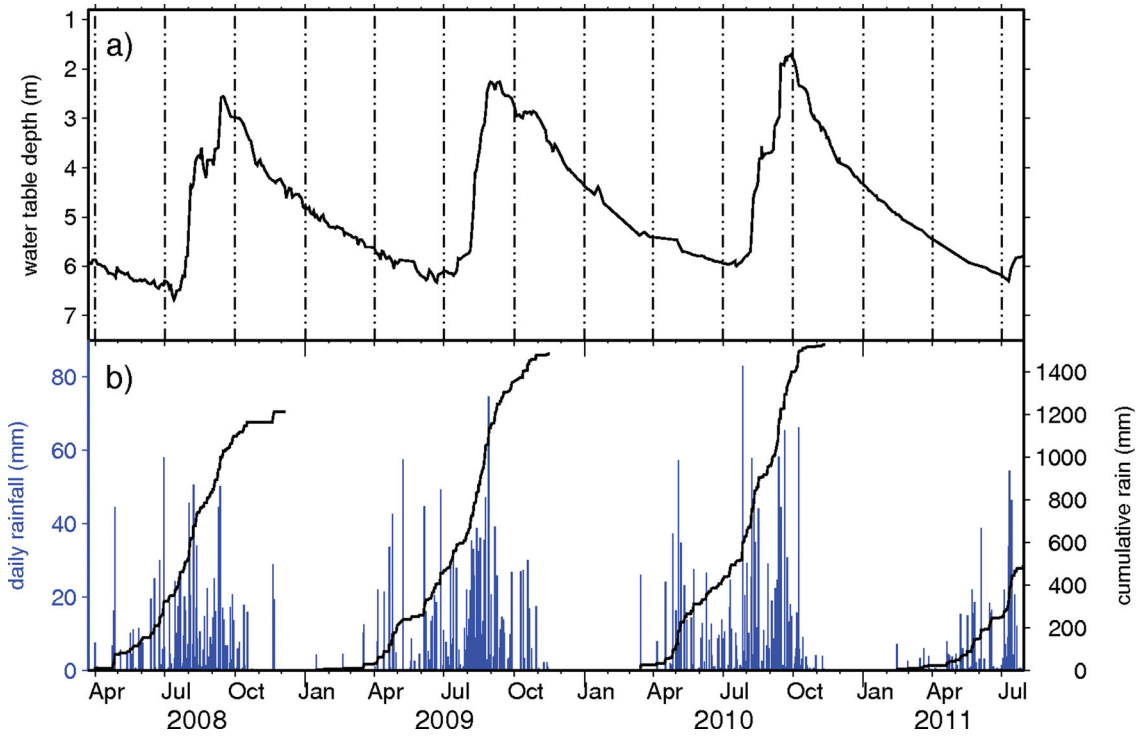

Figure 2. Hydrological data. (a) Water-table time-series. (b) Rainfall data: daily (blue) and cumulative (black). There is a gap in the rainfall data in 2011 May, but regional data show a deficit with respect to past years.

soil moisture. Water contents were obtained by weighting drilling residuals from each depth (i.e. 0.15, 0.3, 0.5 m and every 0.5 m down to 7.5 m) during the drilling process to avoid any loss of water, and by further weighting these samples (about 100 cm^3) after they have been dried in an oven. Dry bulk densities were obtained from gamma-probe measurements at same depths and were used to get volumetric water contents. After each drilling, a 63-mm diameter PVC access tube (enclosed at its bottom) was tight fitted into the borehole (65 mm diameter). The eventual thin gap between the tube and the surrounding soil was filled with fine drilling cuttings. NP measurements were undertaken immediately after the drilling, at the end of the day and the following day. This was done to check if there was no further evolution of the CRs after the drilling, may be due to the closing of some cavities around the access tube in soft areas. If none was detected, and no rain happened in between, the CR associated with the calibration was the mean of the three measurements. After calibration, WSC[L] are deduced from the NP moisture variations ($\Delta\theta$) using the formula

$$\mathrm{WSC} = l\Delta\theta, \tag{2}$$

where $l[L]$ is the investigated thickness (IAEA 2003).

Calibration curves are inferred from recent drillings of about 33 boreholes in 2011 April (dry season), and subsequent calibration drillings in following September (wet season), resulting in 775 (CR, θ) couples. These couples have been associated to three qualitatively defined textural classes based on drill logs analysis. The calibration curve has been inferred for each class, based on the assumption that in such a heterogeneous medium (weathered hard rock), equivalent physical properties can be defined for major units. The three different classes are: soil, lateritic layers and alterite. Classification of each layer has been undertaken qualitatively according colour and texture of cuttings (Fig. 3a).

Statistical parameters of the regression analysis for each class have been used to calculate error estimations on water storage variations, following an approach that takes into account covariance terms between horizons that have the same calibration curve (Vandervaere *et al.* 1994). The total variance σ^2(WSC) of storage variations inferred from NP measurements between two dates is given by

$$\sigma^2(\mathrm{WSC}) = \sigma_{\mathrm{I}}^2(\mathrm{WSC}) + \sigma_{\mathrm{c}}^2(\mathrm{WSC}) + \sigma_{\mathrm{int}}^2(\mathrm{WSC}), \tag{3}$$

where σ_{I}^2(WSC), σ_{c}^2(WSC) and σ_{int}^2(WSC) are the total variance on, respectively, the instrument measurement, the calibration and the integrative method used to interpolate between investigated depths (here we use the trapezoidal method).

NP calibration is based on a linear relationship between counting rates [CR(%)] and water content [θ(%)]:

$$\theta = a + CR \cdot b. \tag{4}$$

4.2 Results

Calibration results are shown in Table 1. Corresponding regression analysis is shown in Figs 3(b)–(d) for each class. Only the borehole close to the gravimeter is used in this study because others are too recent and do not cover the time period of the study.

Soil moisture evolution is shown on Fig. 4, together with the water-table level and daily rainfall. High frequency variations (up to a few days) are not present because of the sampling rate of NP measurements (about 1 week, with some gaps). After a rain event, the top soil rapidly dries out, by evapotranspiration and infiltration. Top soil moisture increases when the first consequent rains fall and water-table rise when water infiltrates deep enough, with a time lag of up to 3–4 months (e.g. the increase in NP-derived

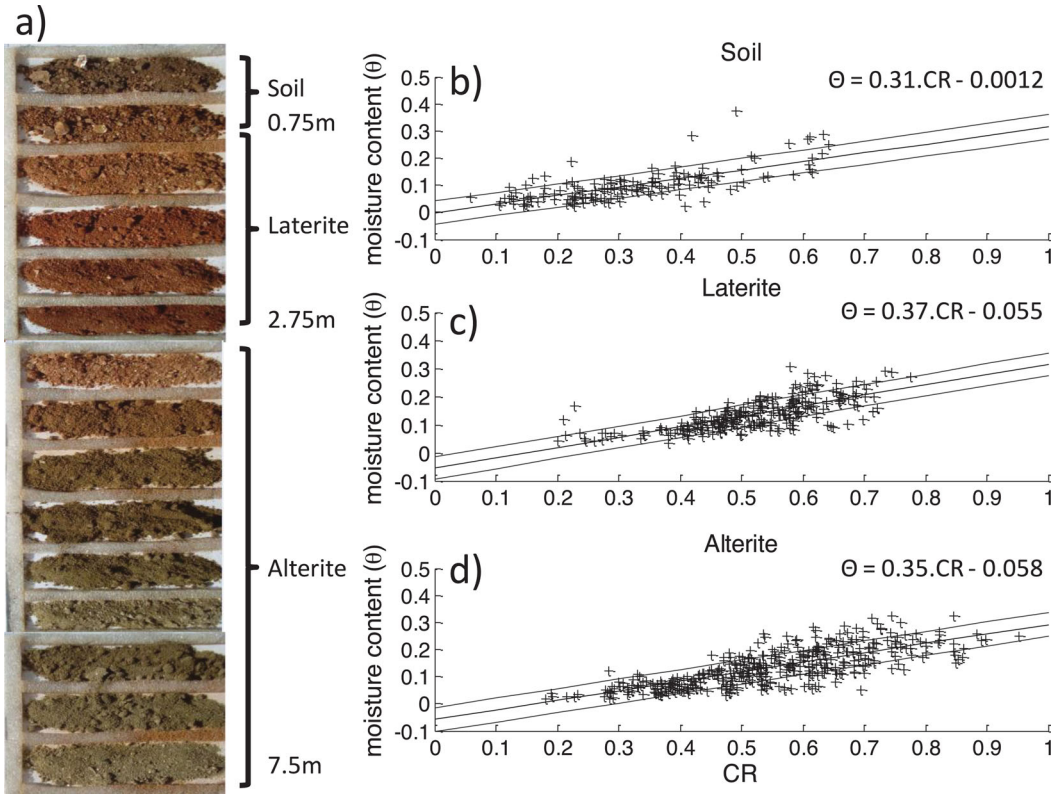

Figure 3. (a) Drilling log of the NP borehole and (b), (c) and (d) calibration regressions for each layer. Dotted lines represent the 1σ confidence interval.

Table 1. Results of NP calibration for each class. m is the number of couples used for calibration, using the equation $\theta = a + CR{\cdot}b + e\sigma(CR,\theta)$ is the covariance between counting rates (CR) and moisture contents (θ), $\sigma^2()$ are variance terms for each parameter of the regression analysis and $\sigma(a,b)$ is the covariance between a and b.

Type	m	$\sigma(CR,\theta)$	b	a	σ^2(e)	$\sigma^2(b)$	$\sigma^2(a)$	$\sigma(a,b)$
Soil	142	0.0058	3.15^{E}-01	−1.20^{E}-03	1.80^{E}-03	6.76^{E}-04	7.12^{E}-05	−2.19^{E}-04
Laterite	260	0.0045	3.71^{E}-01	−5.54^{E}-02	1.40^{E}-03	4.65^{E}-04	1.24^{E}-04	−2.41^{E}-04
Alterite	373	0.0078	3.51^{E}-01	−5.83^{E}-02	2.00^{E}-03	2.36^{E}-04	7.07^{E}-05	−1.29^{E}-04

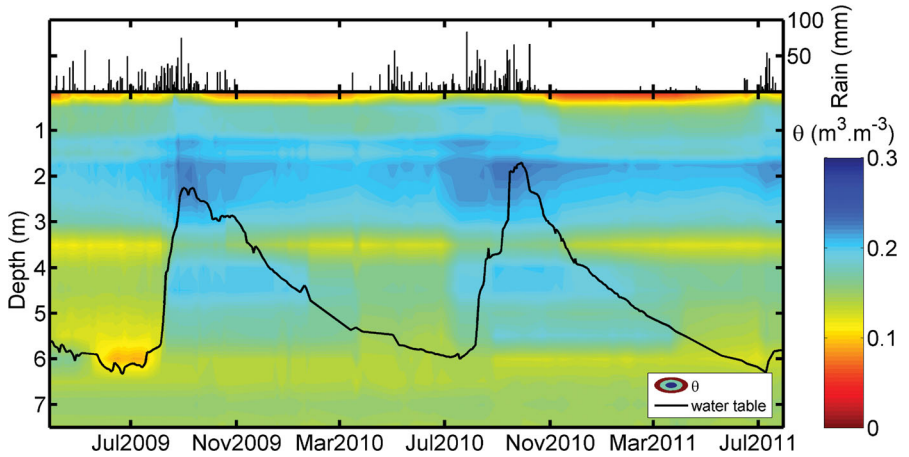

Figure 4. Time-depth evolution of water content derived from NP monitoring. Solid black line is the water-table level and daily rainfall is shown on an independent axis.

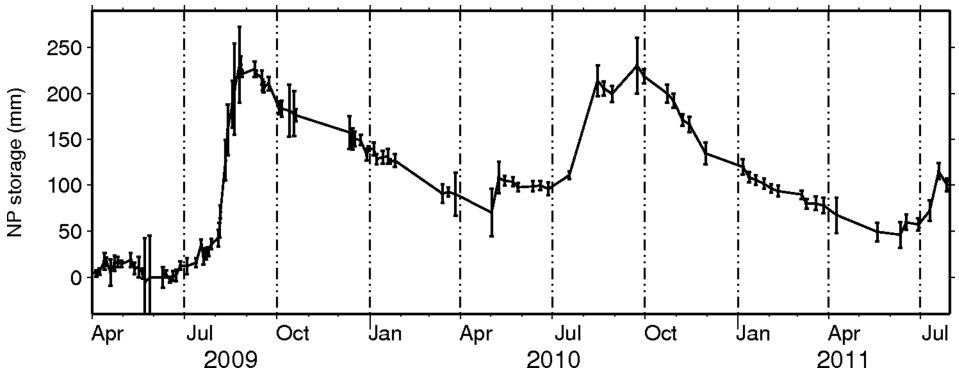

Figure 5. NP derived WSC and associated date-to-date errors.

storage in 2010 May has no obvious consequence on the water-table level). Noise in the data can be observed in the saturated zone, for which water content is supposed to remain constant. The upper part of the profile exhibits a higher water content, as can be expected from this weathered hard-rock basement context. During the dry season, storage variations in the WTFZ (i.e. below 1.7 m) are related to drainage process as evidenced by the analysis of suction data from nearby tensiometers. The two recession periods (from 2009 September to 2010 May and from 2010 September to 2011 July) produce seasonal WSC in the WTFZ of 117 and 125 mm, respectively. Once divided by the associated thickness, this gives average water content variations of 2.8 and 2.9 per cent, respectively. Because water content variations in the WTFZ during these recession periods are caused by drainage process, these values provide an estimate of vertically averaged Sy value at the NP location.

WSC shown on Fig. 5 are cumulative storage variations with respect to the first value that is set to 0. Error bars are calculated on a date-to-date storage variations basis. Standard deviation for WSC is in average 11.6 mm of equivalent water height when all possible couples of the time-series are analysed statistically, and is largely coming from the integration error (Table 2).

Table 2. Mean standard deviations of WSC from NP measurements: σ(WSC), σ_I(WSC), σ_c(WSC) and σ_{int}(WSC) are mean standard deviations on respectively the derived WSC, the instrument measurement, the calibration and the integrative method used to interpolate between investigated depths (here we use the trapezoidal method).

σ(WSC)	σ_I(WSC)	σ_c(WSC)	σ_{int}(WSC)
11.6 ± 10 mm	0.16 ± 4.10^{-3} mm	0.6 ± 0.4 mm	11.6 ± 10 mm

NP data show seasonal WSC (Fig. 5) ranging from about 150 mm for the wet season in 2010 to 250 mm in 2009. In this direct recharge context, the onset of the humid period is seen earlier in the NP data than in the water-table record.

5 RESISTIVITY AND MRS SURVEYS

For delineating structures of the subsurface in the surroundings of the gravimeter, Descloitres *et al.* (2011) have surveyed a 300 × 300 m^2 area using surface geophysical methods. To summarize this study, each geological formation and their respective weathered layers have been identified using a geological survey, resistivity methods and several MRS. Apparent resistivity mapping has been achieved using a Schlumberger array profiling survey with electrode spacing of 20 m, allowing to associate the mapping to the shallowest part of the aquifer. The apparent resistivity map is shown in Fig. 6. Apparent resistivity displays strips with a North–South orientation indicating roughly a 2-D spatial distribution of the corresponding weathered formations. Very clayey zones (conductive) are present jointly with more resistive ones, attributed to low weathered rocks. Because the water content is difficult to quantify with resistivity only, the strips have been investigated using MRS in order to characterize their MRS properties.

The MRS method is based on the property of the nuclei of the hydrogen atoms (protons) in water molecules to have a magnetic moment that can be excited with an alternative magnetic field generated by loop cable laid out on the surface. When the applied field is cut off abruptly, the protons go back to their initial position. Doing so, they generate a relaxation secondary magnetic field, recorded by the instrument. This is the measurement principle of MRS method detailed in numerous publications (see e.g. Legchenko & Valla 2002). The geophysical parameters derived after interpretation are the MRS water content, θ_{MRS}, and the relaxation times, T_2^* and T_1, versus depth. θ_{MRS} is defined as the volume of water per unit volume with decay time constant higher than 30 ms (Legchenko *et al.* 2002). Signal from very clayey formations with too short decay time constants (bound water) are not recorded. θ_{MRS} can give an estimate of the effective porosity, if dead-end and unconnected pores can be neglected (Lubczynski & Roy 2005). Both T_2^* and T_1 are linked to the mean pore size containing water (Kleinberg 1996; Kenyon 1997; Legchenko & Valla 2002). The location of MRS loops (8-shaped geometry due to noise removal procedure) is shown in Fig. 6. MRS show θ_{MRS} values ranging from 1.5 to 10 per cent in the study area, enlightening the strong spatial heterogeneity of the medium (Descloitres *et al.* 2011). Thus, it has been learnt from this survey that *Sy* could vary a lot from place to place and this spatial variation should be considered instead of a 1-D layered subsurface while analysing the gravimeter signal.

6 GRAVITY MONITORING

Absolute gravity measurements were done on a concrete pillar of 1 m^3, uncoupled with the shelter basement. The apparatus settings, measurements protocol and applied corrections are the same as presented by Pfeffer *et al.* (2011). Several series of data sets, each one consisting of 100 drops of the corner cube every 10 s, produce raw gravity values that are corrected for temporal effects, and averaged. Corrections include solid earth tides (tidal parameters from ETGTAB software; Wenzel 1996), ocean loading (Schwiderski 1980), air pressure effects (using barometric *in situ* measurements, and a regression coefficient of -0.3 μGal hPa^{-1}) and polar motion contribution from pole positions given by the international earth rotation service, IERS (http://www.iers.org).

At short timescales, the earth can be considered as an elastic body, hence WSC produce two main effects (Farrell 1972; Jacob 2009): (i) a direct Newtonian effect from the attraction of masses, (ii) elastic deformation. The latter implies two effects on the earth gravitational field: a free-air effect from the radial displacement of the observation point and global mass redistributions. In order to evaluate local WSC (and compare results to local hydrological monitoring), we need to correct gravity data for the non-local contribution. Following Pfeffer *et al.* (2011), we evaluate large-scale effects using the Global Land Data Assimilation System (GLDAS/Noah) model by Rodell *et al.* (2004). We use soil moisture (from surface down to 2 m depth), snow and canopy water outputs provided with 3 hr and 0.25° temporal and spatial resolutions, and over all continental surfaces. The convolution of these global soil water content estimations with the Green's functions for Newtonian and deformation responses on a spherical non-rotating, elastic and isotropic (SNREI) Earth model gives the total gravity variations (Boy & Hinderer 2006). These calculations, together with atmospheric and oceanic loading, can be found in Boy (2012) for the Global Geodynamics Project (GGP) sites, including

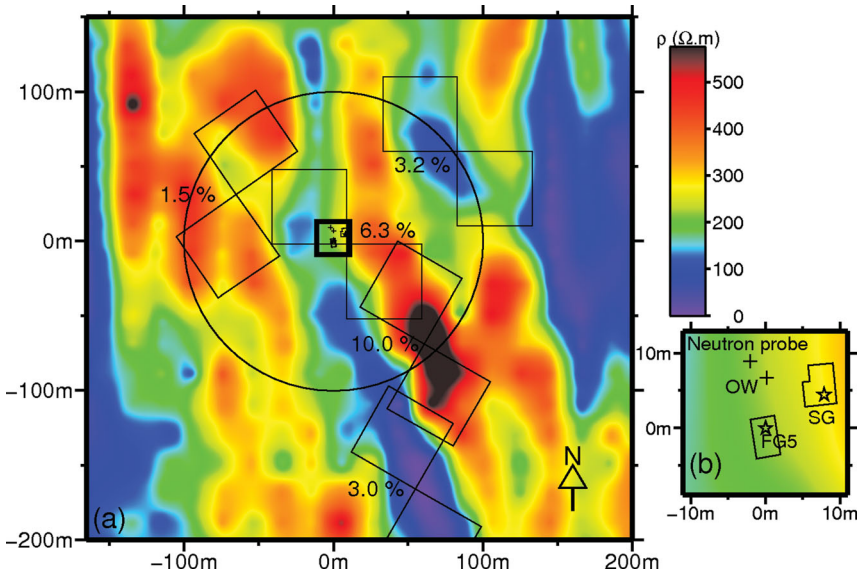

Figure 6. Geophysical data: apparent resistivity mapping and MRS measurements. Numbers are MRS water contents θ_{MRS}. The circle shows the 100-m radius zone of influence for gravity variations at the FG5 site. MRS soundings are 8-shaped cable square loops.

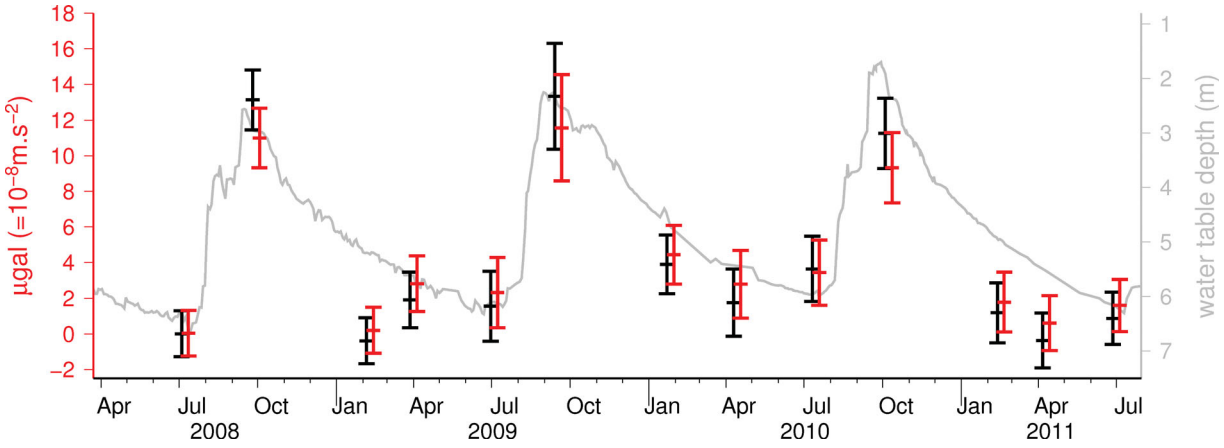

Figure 7. FG5 gravity data: raw (classical corrections applied) data in black, corrected for non-local contribution in red. Absolute values are obtained by adding 978033590.4 µGal. In background and light grey is water-table depth, plotted on an independent axe.

Nalohou. Permanently ice-covered areas (Greenland, Alaska and mountain glaciers) have been masked out and the conservation of the total water mass has been enforced by adding/removing a uniform oceanic layer compensating any lack/excess of water over land. As described in Spratt (1982) or De Linage *et al.* (2007), the Green's functions have a Newtonian term (the direct attraction of the load) and an elastic, deformation-induced term. The former is also the sum of two contributions, local and global. The local term is equal to the Bouguer analytical expression (i.e. see eq. 5 in the next section). The contribution of continental water storage within a range of a several tens of kilometres around the station is negligible if we assume a thin layer load acting on a spherical earth. In this case, the water masses are at a similar height than the gravimeter, and the vertical attraction is almost null (Llubes *et al.* 2004). We correct gravity observations for the non-local contribution, by convolving the corresponding Green's functions with the outputs of the GLDAS/Noah global hydrology model.

Gravity measurements started in 2009 July, with a rate of four measurements per year. Dates have been selected according to the hydrological cycle: at the end of June and early July, the water table is the lowest. The corrected gravity values and associated standard deviation during 3 yr from 2008 July to 2011 July are presented in Fig. 7, together with their values corrected for the non-local hydrological component. As shown by a recent study in Niger, the local and non-local hydrology contributions are in phase, the non-local one being about 20 per cent of the total effect (Pfeffer *et al.* 2011). Hence, the correction for the non-local hydrology reduces the amplitude of gravity variations of local origin. In the background of Fig. 7 is shown the water-table depth, on an independent axis. This allows to roughly compare the phase of the two signals: when groundwater recharge occurs (between July and September), there is a strong increase in gravity (around 10 µGal). One sees mainly the seasonal term since the lack of higher frequency gravity data sampling avoids finer comparisons.

7 GRAVIMETRICAL MODELING

Direct modelling of the gravitational effect of WSC ($\Delta g[LT^{-2}]$) can be achieved at first order by applying the 'Bouguer plate' model:

$$\Delta g = 2\pi\rho G H, \tag{5}$$

where ρ is the density of water $[ML^{-3}]$, G is the gravitational constant $[L^3M^{-1}T^{-2}]$ and H is the thickness of an infinite water layer $[L]$. This analytical expression can give satisfactory results in the case of a flat topography. In order to account for topographic effects, and for spatial heterogeneity of the specific yield, we use in this study a 3-D prisms model built from the prism equation provided by Leirião *et al.* (2009). The terrain has been discretized in prisms according to the topography using a local DEM (Digital Elevation Model) built from a network of points measured with differential GPS. The density of points is higher close to the gravimeter. DEM accuracy (Table 3) is derived from 1000 sets of control points randomly picked from the data set. In the region spanning 300 m around the SG, mean RMSD of DEMs with grid sizes varying from 5 to 20 m is about 0.1 m. The accuracy decreases with the spatial extent because of the lower density of points. Using this modelling approach, we simulated the effect of a 1-m thick layer of water distributed according to the topography, using 10 × 10-m^2 grid cells and obtained 44.5 µGal at the gravimeter measurement site. This

Table 3. DEM accuracy estimates. Mean and standard deviation values are calculated from 1000 sets of control points for each grid centered on the FG5 point.

Grid size (m)	Spatial extent (m)	Data points	Control points	Mean (RMSD) (m)	Std (RMSD) (m)
5	600	941	100	0.1	0.03
10	600	941	100	0.1	0.02
20	600	941	100	0.12	0.02
40	600	941	100	0.17	0.03
5	2000	2447	100	0.31	0.06
10	2000	2447	100	0.34	0.07
20	2000	2447	100	0.448	0.08

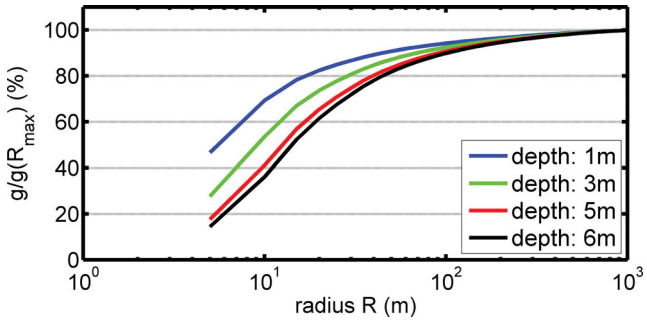

Figure 8. Ratio between the gravity effect of a 1 m layer of water in a disk centred on the FG5 with increasing radius and the gravity effect of a 1 m layer of water in a 2000-m diameter disk. Results are shown for different depths.

is slightly more than the 42 μGal derived from the Bouguer plate analytical expression, implying a small role (about 6 per cent) of the topography with respect to a flat model. The effect of the topography, in this case, results in a higher gravity variation than for the Bouguer plate. This is because the gravimeter is located on top of a hill, and more masses than in the plane geometry are located 'underneath' the gravimeter, thus increasing the vertical component affecting the gravity measure. For instance, Creutzfeldt *et al.* (2008) found a higher value of 52 μGal for SG Wettzell observatory in Germany. The gravity effect of a 1-m thick layer of water at 1, 3 and 6 m deep with respect to the topography has been calculated with different grid sizes (5, 10, 20, 30 and 40 m) from the same DGPS data set. Discrepancies in gravity never exceed 2 per cent between all different grid sizes (largest discrepancies being between the 5 m and the 40 m). This very high accuracy obtained even with coarse grids is due to the very flat terrain, with almost no high frequency variations.

The 100-m footprint area of the gravimeter, such as shown on Fig. 1a, is calculated from the ratio between the gravity effect of a 1 m layer of water in a disk centred on the FG5 with increasing radius and the gravity effect of a 1 m layer of water in a 2000-m diameter disk. This is shown on Fig. 8. 90 per cent of the signal modelled up to a radius of 1000 m come from a disk of 40 m for the 1-m deep layer of water (2.5 m below the FG5), 60 m for the 3-m deep layer of water (4.5 m below the FG5), 80 m for the 5-m deep layer of water (6.5 m below the FG5) and 85 m for the 6-m deep layer of water. The 100 m radius corresponds to 92 per cent of the signal modelled up to a radius of 1000 m for the 5-m deep layer of water, which is about the average water-table level.

This model has been applied for the two goals of the present study: (i) to compare and cross-validate NP and FG5 data; (ii) to account for spatial heterogeneity of the specific yield.

7.1 Error assessment

In the following, the relevance of the fit between observed (Δg_{FG5}) and modelled (Δg_m) gravity variation is assessed using the RMSD equation

$$\mathrm{RMSD} = \sqrt{\frac{\sum_{i=1}^{n}(\Delta g_{\mathrm{FG5},i} - \Delta g_{m,i})^2}{n}}, \tag{6}$$

where n is the number of available time steps.

Variances on observed absolute gravity values are obtained from the distribution of hourly set values for each experiment. Variances on gravity variations are obtained from the summation of respective variances for consecutive data points.

8 JOINT ANALYSIS OF DATA SETS: METHODS

8.1 Comparison of NP and FG5 data

Because NP measurements are made in a single borehole, a 1-D geometry is applied in the first step of this modelling approach. Water content measurements by NP in the 0–7.5 m layer are uniformly applied for each grid cell of the model, accounting for topography. Let $G[\mathrm{WSC}(t)]$ be the transformation of the storage variations through time to gravity variations. Hence,

$$\Delta g_m(\Delta t) = G\left[\mathrm{WSC}_{\mathrm{NP}(0-7.5m)}(t)\right], \tag{7}$$

where $\mathrm{WSC}_{\mathrm{NP}(0-7.5m)}(t)$ are the storage variations measured by NP through the whole vertical profile where storage variations actually occur, and Δg_m is their modelled gravity effect. The latter is compared to FG5-derived gravity variations, and relevance of the fit is evaluated with the RMSD (eq. 6).

The instrument is protected by a 12 m^2 shelter. This modifies the local infiltration in the vicinity of the instrument ('mask effect'), and consequently the lack of close infiltration has been evaluated. This mask effect is taken into account by considering two extreme cases, (i) no soil moisture variations underneath the shelter, or (ii) they are exactly the same as without shelter. The first case is obtained by subtracting to the total modelled signal the gravity effect from WSC occurring underneath the shelter.

One should keep in mind that FG5 measurements are spatially integrated, while NP produces point-measurements. The 1-D assumption made here can be inappropriate because 2-D structures have been evidenced with surface geophysics.

Error assessment

The confidence interval on modelled gravity variations is simply calculated as the gravity effect of the NP-derived storage time-series; with $\pm 1\sigma$ uncertainty in NP values (as shown on Fig. 5, calculated using eq. 3).

8.2 2-D model for specific yield

The water-table fluctuations can be considered as representative over the 100 m radius around the FG5 site, as confirmed by the similarity exhibited by different water-table measurements carried out close to the site. Considering water-table fluctuations in the saturated zone of the model allows hence to account for spatial variability of the storage through Sy mapping. For unconfined aquifers, mass variations in the saturated zone are directly linked to the specific yield. Its value and spatial distribution control the amount of water that produces gravity variations (Pool & Eychaner 1995). A 2-D model for θ_{MRS} is shown in Fig. 9. Cells size is 20 × 20 m^2 large in the vicinity of the gravimeter and 50 × 50 m^2 further away. Taking smaller cells had no influence, because of the relatively flat topography (see Section 7). Also, the resolution of resistivity mapping is not precise enough to describe a possible structure for θ_{MRS} at finer scales.

Numerous studies showed that θ_{MRS} is somewhat different from Sy (Vouillamoz *et al.* 2005; Boucher *et al.* 2009; Vouillamoz *et al.* 2012) and rather close to the effective porosity, defined as the portion

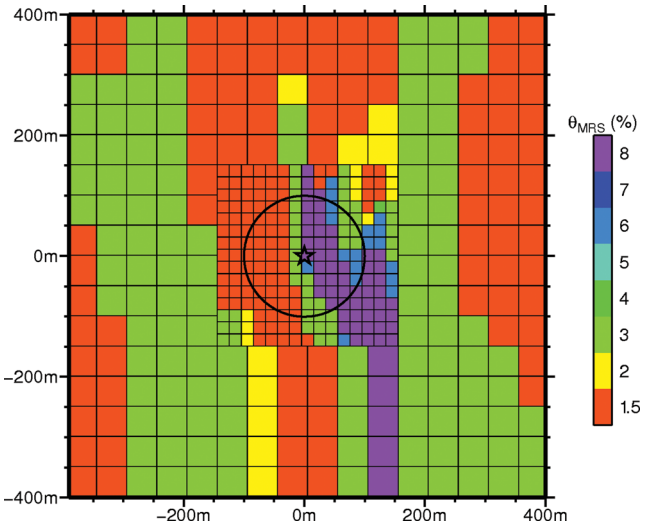

Figure 9. 2-D model for θ_{MRS} obtained through the spatialization of MRS water contents using resistivity mapping and geological observations. The circle shows the 100-m radius zone of influence for the FG5 gravimeter.

of a medium that contributes to the flow and advective transport (Lubczynski & Roy 2005). Knowing this, we scaled the 2-D model by a factor α, using

$$Sy = \alpha\theta_{MRS}(x, y), \tag{8}$$

where $\theta_{MRS}(x, y)$ stands for the spatial distribution of the MRS water content.

Gravity variations from the WTFZ and the VZ are modelled by

$$\Delta g_m(\Delta t) = G\left[\Delta h \alpha \theta_{MRS}(x, y) + \mathrm{WSC}_{NP(VZ)}(t)\right], \tag{9}$$

where Δh is the water-table variations uniformly distributed according to the topography. It is then possible to optimize the α parameter (eq. 9) with respect to FG5 data, minimizing the RMSD (eq. 6).

It is also possible to derive a 1-D equivalent Sy parameter, by adjusting a single value of Sy over the whole area without taking into account the spatial variability. To derive a 1-D equivalent Sy value is highly interesting for hydrological models, or for any further attempt to use gravity data as a proxy for water storage monitoring.

8.3 Error assessment

Variances on modelled gravity variations are estimated for the two contributing compartments (WTFZ and VZ). For the WTFZ, water-table measurements can be considered to be quite accurate. If we hypothesize an uncertainty of 1 cm on the reading, with an average Sy value of 5 per cent, this leads to a 0.5 mm error on storage estimation, which is insignificant compared to NP measurements errors (as shown on Table 2). However, spatial variations of the water table in the vicinity of the gravimeter site are not taken into account in this study. As specified in Section 3, other boreholes exhibit similar variations, and discrepancies seem not to be correlated to spatial variations of θ_{MRS}, as one could expect a correlation between water-table levels and Sy. For the VZ (the 0–1.7 m layer), standard deviations on NP-derived storage variations are obtained using eq. 3. Then, their gravity effect has been calculated using the present model.

To get the best-fitting α value, a simple Monte–Carlo approach is adopted: 40 000 sets of (modeled VZ gravity contribution, observed FG5 data) scattered couples are randomly sampled within their distribution in both dimensions, assuming they are normally distributed. These distributions are defined by their mean values and standard deviations based on the error assessments of observed gravity variations and modelled VZ contributions. For each set, the contribution of the WTFZ is added by testing a range of α values. The best-fitting α for each set is found by minimizing the RMSD (eq. 6). We eventually obtain both the mean value and standard deviation of the resulting α distribution.

9 JOINT ANALYSIS OF DATA SETS: RESULTS

9.1 1-D model: cross-validation of NP and FG5 data

The first result of this study arises from the comparison of gravity data with direct water content measurements by NP in the 0–7.5 m layer (the whole profile where WSC occur), from which the gravity effect is calculated using the aforementioned model (Fig. 10). In this figure, as we are dealing with storage variations, each modelled time-series is vertically shifted with an offset that minimizes the distances to FG5 data points. When considering the mask effect of the shelter (i.e. no WSC underneath the shelter), the

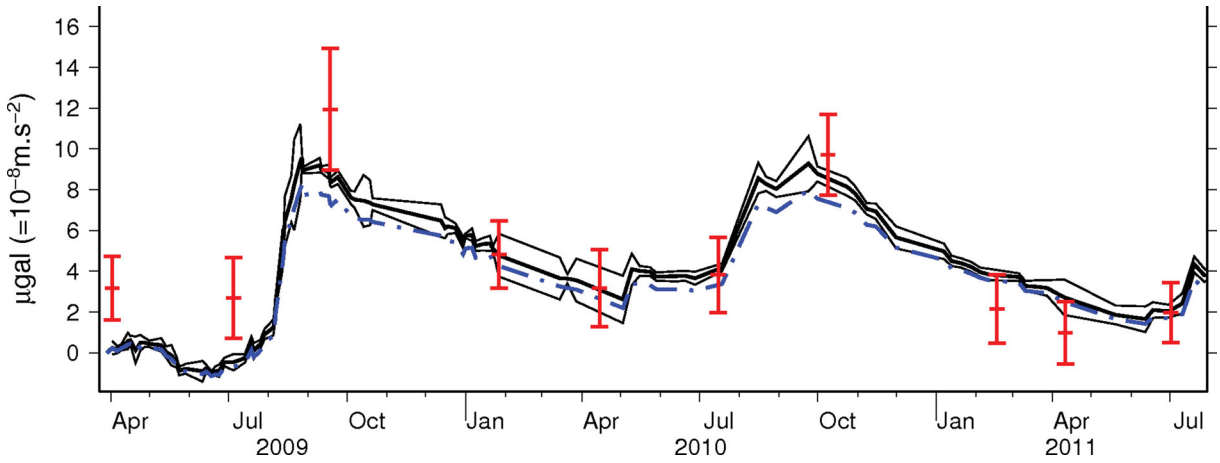

Figure 10. FG5 data (red points with error bars) and gravity modelling of NP-derived storage variations (black line). Light black curves show the confidence interval at $\pm 1\sigma$. Dashed blue curve takes into account the mask effect of the shelter (i.e. no WSC underneath the shelter).

calculation produces a time-series that remains most of the time within the error bars of the former (blue curve in Fig. 10). The comparison shows a fair agreement when considering respective error bars (RMSD = 1.61 μGal). Discrepancies between gravity measurements and the water storage model made out of point measurements can be related to the non-representativeness of the NP data (point measurements in a specific borehole) with respect to the larger zone 'seen' by the gravimeter. This is particularly true in case of strong local heterogeneities. Hence, the next step is to introduce the spatial distribution of θ_{MRS}, known to be close to Sy.

9.2 2-D model and specific yield estimation

Fig. 11 shows the results of the 2-D model for specific yield (black curve), derived from MRS and resistivity mapping, assuming that $\theta_{MRS} = Sy$ (i.e. $\alpha = 1$). The gravity data, within their standard deviation, are not so well adjusted to the modelled water storage variations, particularly for the 'wet' point in 2010 and the two points in 2009 April and July. The black curve comes from the summation of two contributions, the VZ and the WTFZ. Relative contributions from the VZ and the WTFZ are 20 and 80 per cent, respectively, enlightening that now 80 per cent of the model does account for spatial heterogeneities of the specific yield. Furthermore, the underlying assumption of spatial homogeneity in the upper (VZ) layer needs to be valid in a smaller area (see Fig. 8). The RMSD of the fit is 2.5 μGal, and associated scatter plot is shown on Fig. 12(a) (black points). Recent data from six other NP boreholes located within the 100 m radius of influence of the gravimeter indicated a mean seasonal amplitude in the VZ of 74 ± 10 mm for the 2011–2012 hydrological year. This standard deviation of 10 mm of equivalent water thickness corresponds to 0.44 μGal when using the linear relationship of 0.044 μGal mm^{-1} (see Section 7). This is small compared to the seasonal signal, and to the RMSD of the fit, assuming little impact of using a single borehole for the VZ.

The WTFZ can produce the same contribution if we consider a uniform model of $\theta_{MRS\_equ1\text{-}D} = 0.07$. This value is retrieved by assuming an homogeneous layer with a constant specific yield value in the WTFZ, and testing a range of values until the same curve as the one coming from the spatial model $\theta_{MRS}(x, y)$ with $\alpha = 1$ (Fig. 11) is qualitatively found (i.e. results with $= 1$ are exactly the same as when using a uniform layer with $Sy = 0.07$). This value can be seen as an averaged θ_{MRS} within the footprint area of the gravimeter, somehow weighted by an inverse square distance function.

When using the 2-D model (eq. 9), it is thus possible to find the optimal α value, with respect to gravity data, by minimizing the RMSD (eq. 6). Results are shown on Fig. 11 (blue line) for the time-series, and on Fig. 12(a) (blue points) for the fit between

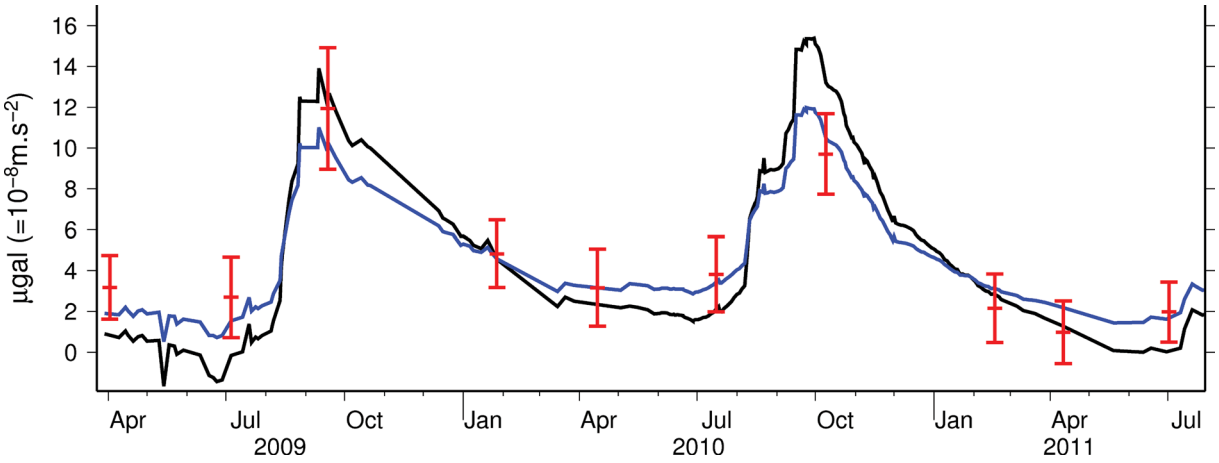

Figure 11. FG5 data (red points with error bars) and gravity modelling of hydrological effect: black and blue curves are the sum of the VZ contribution and the WTFZ contribution with respectively the spatialized θ_{MRS}, with $\alpha = 1$ (black), or with the best-fitting α value (blue).

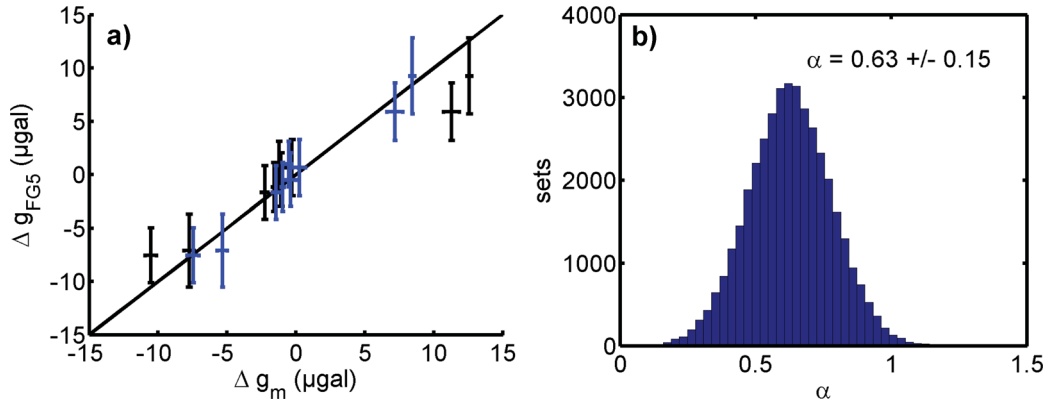

Figure 12. (a) Scatter plot of gravity variations (model and data) for both the distributed model $\theta_{MRS}(x, y)$ with $\alpha = 1$ (black points) and the best-fitting α value (blue points) and respective error bars. (b) Distribution of optimized α values for the 40 000 sets of (modelled VZ gravity contribution, observed FG5 data) scattered couples.

observed and modelled gravity variations. Blue points are closer to the $y = x$ line than black points, with a RMSD value of 0.94 μGal. They show a better agreement with FG5 data than both the spatial $\theta_{MRS}(x, y)$ ($\alpha = 1$) model and the 1-D uniform (NP) model.

The distribution of best-fitting α values following the Monte Carlo sampling scheme is shown on Fig. 12(b). Results seem normally distributed, and mean α value is 0.63 with a standard deviation of 0.15.

10 DISCUSSION

10.1 Storage variations

For the first time, gravity variations are compared to WSC measured by NP through the whole vertical profile, including the WTFZ. Integrative (100 m radius) gravity measurements show a good fit with modelled gravity from NP point measurements under the 1-D uniform assumption. Discrepancies between modelled and observed gravity variations (RMSD = 1.61μGal) may arise from the strong heterogeneity of the investigated medium. The modelled shelter effect (no WSC underneath the shelter) provides a time-series that is very close to the unmasked one. Furthermore, because we focus on the seasonal scale (3 months sampling rate for the FG5 data), it is very likely that redistribution of water underneath the shelter occurs, minimizing this mask effect.

However, both time-series fit within their own error bars, providing us with a new validation of gravity data potential for hydrological studies. This validation of WSC quantification using absolute gravity data allows some comparisons with previous studies. For instance, daily gravimetric decrease rates during the dry season (deduced from gravimetric measurement in September and January) are of about $0.05 - 0.08$μGal d^{-1}, that is to say, $1.1 - 1.8$mm d^{-1}. This is in fair agreement with evapotranspiration values obtained during the dry season by scintillometry (Guyot *et al.* 2009), or by hydrological budget studies (Séguis *et al.* 2011) on this same study area, but with a microbasin wide (22.6 ha) spatial extent. Also, gravity data give us information about the interannual storage variations: minimum storage increased from 2008 to 2010 (1.7 ± 1.1μGal yr^{-1}), comparatively with water-table levels (Fig. 4), and resulting from 2 wet years.

10.2 Specific yield and MRS water content

An attempt to account for spatial heterogeneity of specific yield has been made on the basis of MRS and resistivity mapping. A single gravity time-series is in no way able to constrain such a spatial distribution. However, the lower RMSD value (Table 4) of this approach, with respect to the 1-D assumption, seems to confirm the interest of the method that combines hydrological data and geophysical survey for retrieving WSC.

Deriving the best-fitting α parameter means retrieving the $\alpha = Sy/\theta_{MRS}$ ratio for the footprint area of the gravimeter, somehow weighted by an inverse square distance function. Vouillamoz *et al.* (2005) for crystalline basement aquifers in Burkina Faso and Boucher *et al.* (2009) for sedimentary aquifers in SW Niger showed that θ_{MRS} was higher than Sy obtained by pumping tests. The latter experiment has been confirmed by Pfeffer *et al.* (2011) when they compared MRS data and Sy from gravity monitoring. This is because θ_{MRS} is an estimate of the effective porosity rather than specific yield (Lubczynski & Roy 2005). In the clayey weathered rocks of this study, effective porosity should be clearly higher than specific yield and thus θ_{MRS} higher than Sy (Vouillamoz *et al.* 2012). These authors found $Sy/\theta_{MRS} = 0.4$ for a clayey sandstones aquifer in Northern Cambodia. We found that $Sy/\theta_{MRS} = 0.63 \pm 0.15$ thus confirming previous results. The 1-D equivalent Sy value for each model are shown on Table 4, and are consistent with the best-fitting α value ($\alpha = Sy/\theta_{MRS} = 4.4/7 = 0.63$). Thus, a 1-D equivalent value of 4.4 per cent is to be kept for the footprint area of the gravimeter. This value can be compared to Sy values derived from NP and water-table monitoring (see Section 4) during the two recession periods: 2.8 and 2.9 per cent, although these are only valid locally. Furthermore, both approaches have the limitation of producing a vertically averaged value, which has practical interests for hydrogeologists, but that may differ from the Sy of single layers. This 1-D equivalent approach will serve further hydrological modelling, and will be employed to monitor groundwater storage from gravity data onsite.

10.3 Perspectives

Scarce absolute gravity data have proven to provide reliable estimations on both water storage variations and specific yield estimates when used jointly with complementary hydrological data. A SG is available on site since the summer of 2010 and provides us with a high precision (≈0.1 μGal) continuous time-series of gravity variations. Because of a strong initial drift in this relative gravimeter, data were not available for the timespan of this study. However, they will be used to achieve a precise monitoring of water storage variations, both at seasonal scale and short timescale (rainfall event). Also, microgravity relative measurements are currently undertaken to extend this data intercomparison to the small catchment surrounding the FG5 site. They will be used to infer spatiotemporal variability of recharge processes, and hopefully validating repeated microgravity measurements for hydrological processes studies at the catchment scale. They will also allow to further check the 2-D model of θ_{MRS} described in this study.

As gravity observations allow to recover seasonal storage variations, they can effectively be used for recharge monitoring. This study is currently undertaken, together with an analysis derived from these field experiments to recover the time variability of the specific yield. The field of hydrogravimetry proves to bring further

Table 4. RMSD, correlation coefficient and p value between observed and modelled gravity variations for each model, and 1-D equivalent Sy for both the $\alpha = 1$ and the best-fitting α model.

Model	1-D NP	2-D $\theta_{MRS}(x, y)(\alpha = 1)$	2-D $\alpha = 0.63 \pm 0.15$
RMSD (μGal)	1.61	2.50	0.94
Correlation coefficient	0.97	0.97	0.98
P Value	2×10^{-5}	7×10^{-6}	2×10^{-6}
1-D equivalent Sy (per cent)	–	7	4.4

insights for hydrologists by providing new kind of integrated observations, as long as non-hydrological components can effectively be corrected from the signal.

11 CONCLUSION

In this study, absolute gravity data from FG5 monitoring have been compared to modelled gravity variations derived from WSC measurements by NP and water-table level. Gravity data have been corrected for solid earth tides, ocean loading, air pressure effects, polar motion contribution and non-local hydrology and residuals are associated to local WSC and show seasonal variations of up to 11 μGal. This is somewhat higher than gravity variations deduced from NP only and distributed according to the topography, using a 0.1-m accuracy DEM. NP data have the advantage to investigate the whole profile where WSC occur in this weathered hard-rock basement context. Drawbacks of comparing NP data to gravity data are the local character of the former, with respect to the integrated nature of the second.

Spatial heterogeneities of the WTFZ were taken into account in the second part of this study, by scaling a factor of a 2-D model for θ_{MRS} on the basis of gravity residuals. This resulted in a significant decrease of the RMSD between gravity residuals and the modelled signal and thus militates for the proper modelling of the spatial distribution of WSC, especially in such heterogeneous medium.

ACKNOWLEDGEMENTS

This work has been performed within the frames of the ANR GHYRAF project and the AMMA-CATCH observation system. The authors would like to thank numerous people who helped to achieve this work. Calvo M., Bernard J.D., and Tahirou Sarè for FG5 measurements, Imorou I., Pagou E., Ouani T., Afouda S., for hydrological acquisition, and Ferhat G. for topographic mapping. We would also like to thank the project partners who allowed the use of their infrastructure and provided valuable information and advices. From the Direction Générale de l'eau (DG-Eau, Cotonou): Gbodogbé J.C. and Zannou A., from the Abomey-Calavi university: Yalo N. Creutzfeldt B. and another anonymous reviewer deserve a special mention for the very complete and constructive review that significantly helped to improve the present paper.

REFERENCES

Achidi, J.B., Bourguet, L., Elsaesser, R., Legier, A., Paulvé, E. & Tribouillard, N., 2012. *Carte hydrogéologique du Bénin,* 1:500 000, Ministère de l'Energie, des recherches pétrolières et minières, de l'eau et du développement des énergies renouvelables.

AMMA database, 2013. Available at: http://database.amma-international.org. (last accessed 3 April 2013).

Le Barbé, L., Lebel, T. & Tapsoba, D., 2002. Rainfall Variability in West Africa during the Years 1950–90., *J. Clim.,* **15,** 187–202.

Boucher, M., Favreau, G., Vouillamoz, J.M., Nazoumou, Y. & Legchenko, A., 2009. Estimating specific yield and transmissivity with magnetic resonance sounding in an unconfined sandstone aquifer (Niger), *Hydrogeol. J.,* **17,** 1805–1815.

Bower, D. & Courtier, N., 1998. Precipitation effects on gravity measurements at the Canadian Absolute Gravity Site, *Phys. Earth planet. Int.,* **106**(3–4), 353–369.

Boy, J.-P., 2012. GGP loading. Available at: http://loading.u-strasbg.fr/GGP/10.1093/gji/ggt146.html. Accessed 1 April 2013.

Boy, J.-P. & Hinderer, J., 2006. Study of the seasonal gravity signal in superconducting gravimeter data, *J. Geodyn.,* **41**(1–3), 227–233.

Christiansen, L., Binning, P., Rosbjerg, D., Andersen, O.B. & Bauer-Gottwein, P., 2011a. Using time-lapse gravity for groundwater model calibration: an application to alluvial aquifer storage, *Water Resour. Res,* **47,** doi:10.1029/2010WR009859.

Christiansen, L., Haarder, E.B., Hansen, A.B., Looms, M.C., Binning, P., Rosbjerg, D., Andersen, O.B. & Bauer-Gottwein, P., 2011b. Calibrating vadose zone models with time-lapse gravity data, *Vadose Zone J.,* **10,** 1–11.

Creutzfeldt, B., Guntner, A., Klugel, T. & Wziontek, H., 2008. Simulating the influence of water storage changes on the superconducting gravimeter of the Geodetic Observatory Wettzell, Germany, *Geophysics,* **73**(6), WA95–WA104, doi:10.1190/1.2992508.

Creutzfeldt, B., Güntner, A., Thoss, H., Merz, B. & Wziontek, H., 2010a. Measuring the effect of local water storage changes on in situ gravity observations: case study of the Geodetic Observatory Wettzell, Germany, *Water Resour. Res,* **46,** W08531, doi:10.1029/2009WR008359.

Creutzfeldt, B., Güntner, A., Vorogushyn, S. & Merz, B., 2010b. The benefits of gravimeter observations for modelling water storage changes at the field scale, *Hydrol. Earth Sys. Sci.,* **14**(9), 1715–1730.

Descloitres, M., Séguis, L., Legchenko, A., Wubda, M., Guyot, A. & Cohard, J.M., 2011. The contribution of MRS and resistivity methods to the interpretation of actual evapo-transpiration measurements: a case study in metamorphic context in north Bénin, *Near Surface Geophys.,* **9**(2), 187–200.

Direction des études démographiques, 2003. *Recensement de la Population 2003,* Institut National de la Statistique et de l'Analyse Économique, Benin.

Dubus, N. & Dubus, J., 2011. *La sécheresse au Sahel: Vers une gestion concertée,* Hermes Science Publications, Paris.

Farrell, W.E., 1972. Deformation of the Earth by surface loads, *Rev. Geophys.,* **10**(3), 761–797.

Ferré, T. *et al.*, 2009. Critical steps for the continuing advancement of hydrogeophysics, *EOS, Trans. Am. Geophys. Un.,* **90**(23), 200, doi:10.1029/2009EO230004.

Gehman, C.L., Harry, D.L., Sanford, W.E., Stednick, J.D. & Beckman, N.A., 2009. Estimating specific yield and storage change in an unconfined aquifer using temporal gravity surveys, *Water Resour. Res.,* **45,** W00D21, doi:10.1029/2007WR006096.

Goodkind, J.M., 1999. The superconducting gravimeter, *Rev. Sci. Instrum.,* **70**(11), 4131–4152.

Guyot, A., Cohard, J.-M., Anquetin, S., Galle, S. & Lloyd, C.R., 2009. Combined analysis of energy and water balances to estimate latent heat flux of a sudanian small catchment, *J. Hydrol.,* **375**(1–2), 227–240.

Harnisch, G. & Harnisch, M., 2006. Hydrological influences in long gravimetric data series, *J. Geodyn.,* **41**(1–3), 276–287.

Healy, R.W. & Cook, P.G., 2002. Using groundwater levels to estimate recharge, *Hydrogeol. J.,* **10**(1), 91–109.

Healy, R.W. & Scanlon, B.R., 2010. *Estimating Groundwater Recharge,* Cambridge University Press, Cambridge.

Hinderer, J., Crossley, D. & Warburton, R.J., 2007. 3.04—gravimetric methods—superconducting gravity meters, in *Treatise on Geophysics,* pp. 65–122, ed. Schubert, G., Elsevier, Amsterdam.

Hinderer, J. *et al.*, 2009. The GHYRAF (Gravity and Hydrology in Africa) experiment: description and first results, *J. Geodyn.,* **48**(3–5), 172–181.

Hinderer, J. *et al.*, 2012. Land water storage changes from ground and space geodesy: first results from the GHYRAF (gravity and hydrology in Africa) experiment, *Pure Appl. Geophys.,* **169**(8), 1391–1410.

IAEA, 2003. *Neutron and Gamma Probes: Their Use in Agronomy,* IAEA.

Imanishi, Y., Kokubo, K. & Tatehata, H., 2006. Effect of underground water on gravity observation at Matsushiro, Japan, *J. Geodyn.,* **41**(1–3), 221–226.

Jacob, T., 2009. Apport de la gravimétrie et de l'inclinométrie à l'hydrologie karstique, *PhD thesis*, Université de Montpellier II.

Jacob, T. *et al.*, 2008. Absolute gravity monitoring of water storage variation in a karst aquifer on the larzac plateau (Southern France), *J. Hydrol.,* **359**(1–2), 105–117.

Jacob, T., Bayer, R., Chery, J. & Le Moigne, N., 2010. Time-lapse microgravity surveys reveal water storage heterogeneity of a karst aquifer, *J. geophys. Res.: Solid Earth,* **115,** B6, doi:10.1029/2009JB006616.

Kamagaté, B., Séguis, L., Favreau, G., Seidel, J.-L., Descloitres, M. & Affaton, P., 2007. Processus et bilan des flux hydriques d'un bassin versant de milieu tropical de socle au Bénin (Donga, haut Ouémé), *Comptes Rendus Geosci.,* **339**(6), 418–429.

Kenyon, W.E., 1997. Petrophysical principles of applications of NMR logging, *Log Anal.,* **38,** 21–43.

Kleinberg, R.L., 1996. Utility of NMR T2 distributions, connection with capillary pressure, clay effect, and determination of the surface relaxivity parameter $\rho 2$, *Magn. Reson. Imag.,* **14**(7–8), 761–767.

Kroner, C. & Jahr, T., 2006. Hydrological experiments around the superconducting gravimeter at Moxa Observatory, *J. Geodyn.,* **41**(1–3), 268–275.

Le Lay, M. & Galle, S.F., 2005. Variabilités interannuelle et intra-saisonnière des pluies aux échelles hydrologiques. La mousson ouest-africaine en climat soudanien, *Hydrol. Sci. J.,* **50**(3), 509–524.

Lebel, T. *et al.*, 2009. AMMA-CATCH studies in the Sahelian region of West-Africa: an overview, *J. Hydrol.,* **375**(1–2), 3–13.

Legchenko, A., Baltassat, J.-M., Beauce, A. & Bernard, J., 2002. Nuclear magnetic resonance as a geophysical tool for hydrogeologists, *J. appl. Geophys.,* **50**(1–2), 21–46.

Legchenko, A. & Valla, P., 2002. A review of the basic principles for proton magnetic resonance sounding measurements, *J. appl. Geophys.,* **50**(1–2), 3–19.

Leirião, S., He, X., Christiansen, L., Andersen, O.B. & Bauer-Gottwein, P., 2009. Calculation of the temporal gravity variation from spatially variable water storage change in soils and aquifers, *J. Hydrol.,* **365**(3–4), 302–309.

De Linage, C., Hinderer, J. & Rogister, Y., 2007. A search for the ratio between gravity variation and vertical displacement due to a surface load, *Geophys. J. Int.,* **171**(3), 986–994.

Llubes, M., Florsch, N., Hinderer, J., Longuevergne, L. & Amalvict, M., 2004. Local hydrology, the Global Geodynamics Project and CHAMP/GRACE perspective: some case studies, *J. Geodyn.,* **38,** 355–374.

Longuevergne, L., Boy, J., Florsch, N., Viville, D., Ferhat, G., Ulrich, P., Luck, B. & Hinderer, J., 2009. Local and global hydrological contributions to gravity variations observed in Strasbourg, *J. Geodyn.,* **48**(3–5), 189–194.

Lubczynski, M. & Roy, J., 2005. MRS contribution to hydrogeological system parametrization, *Near Surface Geophys.,* **3**(3), 131–139.

MacDonald, A.M., Bonsor, H.C., Dochartaigh, B. & Taylor, R.G., 2012. Quantitative maps of groundwater resources in Africa, *Environ. Res. Lett.,* **7**(2), 024009, doi:10.1088/1748-9326/7/2/024009.

Montgomery, E.L., 1971. Determination of coefficient of storage by use of gravity measurements, in *Department of Geosciences,* University of Arizona, Tucson, AZ, USA.

Naujoks, M., Kroner, C., Weise, A., Jahr, T., Krause, P. & Eisner, S., 2010. Evaluating local hydrological modelling by temporal gravity observations and a gravimetric three-dimensional model, *Geophys. J. Int.,* **182**(1), 233–249.

Naujoks, M., Weise, A., Kroner, C. & Jahr, T., 2008. Detection of small hydrological variations in gravity by repeated observations with relative gravimeters, *J. Geod.,* **82**(9), 543–553.

Niebauer, T.M., Sasagawa, G.S., Faller, J.E., Hilt, R. & Klopping, F., 1995. A new generation of absolute gravimeters, *Metrologia,* **32**(3), 159–180.

Pfeffer, J. *et al.*, 2011. Local and global hydrological contributions to time variable gravity in Southwest Niger, *Geophys. J. Int.,* **184**(2), 661–672.

Pfeffer, J. *et al.*, 2013. Evaluating surface and subsurface water storage variations at small time and space scales from relative gravity measurements in semi-arid Niger, *Water Resour. Res.,* in press, doi:10.1002/wrcr.20235.

Pool, D.R. & Eychaner, J.H., 1995. Measurements of aquifer-storage change and specific yield using gravity surveys, *Ground Water,* **33**(3), 425–432.

Reseau des Bassins Versants, 2013. WordPress, http://rnbv.ipgp.fr/ (last accessed 1 April 2013).

Rodell, M. *et al.*, 2004. The Global Land Data Assimilation System, *Bull. Am. Meteorol. Soc.,* **85,** 381–394.

Scanlon, B., Healy, R. & Cook, P., 2002. Choosing appropriate techniques for quantifying groundwater recharge, *Hydrogeol. J.,* **10**(2), 347–347.

Schwiderski, E.W., 1980. Ocean tides, part II: a hydrodynamical interpolation model, *Mar. Geod.,* **3**(1–4), 219–255.

Séguis, L. *et al.*, 2011. Origins of streamflow in a crystalline basement catchment in a sub-humid Sudanian zone: the Donga basin (Benin, West Africa): inter-annual variability of water budget, *J. Hydrol.,* **402**(1–2), 1–13.

Shamsudduha, M., Taylor, R.G. & Longuevergne, L., 2012. Monitoring groundwater storage changes in the highly seasonal humid tropics: validation of GRACE measurements in the Bengal Basin, *Water Resour. Res.,* **48**(2), doi:10.1029/2011WR010993.

Spratt, R.S., 1982. Modelling the effect of atmospheric pressure variations on gravity, *Geophys. J. R. astr. Soc.,* **71**(1), 173–186.

Van Camp, M., Vanclooster, M., Crommen, O., Petermans, T., Verbeeck, K., Meurers, B., Van Dam, T. & Dassargues, A., 2006. Hydrogeological investigations at the Membach station, Belgium, and application to correct long periodic gravity variations, *J. geophys. Res.,* **111,** B10403, doi:10.1029/2006JB004405.

Vandervaere, J.P., Vauclin, M., Haverkamp, R. & Cuenca, R.H., 1994. Error analysis in estimating soil water balance of irrigated fields during the EFEDA experiment: 1. Local standpoint, *J. Hydrol.,* **156**(1–4), 351–370.

Vouillamoz, J.M., Descloitres, M., Toe, G. & Legchenko, A., 2005. Characterization of crystalline basement aquifers with MRS: comparison with boreholes and pumping tests data in Burkina Faso, *Near Surface Geophys.,* **3**(3), 205–213.

Vouillamoz, J.M., Sokheng, S., Bruyere, O., Caron, D. & Arnout, L., 2012. Towards a better estimate of storage properties of aquifer with magnetic resonance sounding, *J. Hydrol.,* **458–459,** 51–58.

Wenzel, H., 1996. The Nanogal software: Earth tide data processing package ETERNA 3.30, *Bull. d' Inform. des Marées Terrestres,* **124,** 9425–9439.